Check for updates

Flexographic printed microwave-assisted grown zinc oxide nanostructures for sensing applications†

Maria Morais, [ID] [a] Emanuel Carlos, [ID] *[a] Ana Rovisco,[a] Tomás Calmeiro,[a] Hugo Gamboa,[b] Elvira Fortunato, [ID] [a] Rodrigo Martins[a] and Pedro Barquinha*[a]

The development of flexible electronics has increased the demand for wearable pressure sensors that can be used to monitor various biomedical signals. In this context, pressure sensors based on zinc oxide (ZnO) have great potential since, besides the biocompatibility and biodegradability of this metal oxide, it also has piezoelectric properties. The common feature of these sensors is the alignment of the ZnO nanostructures in the strain direction. This alignment is achieved through a three-stage procedure: deposition of a ZnO nanoparticle layer (seed layer) followed by its patterning and the subsequent growth of nanostructures from the seed layer nanoparticles. Herein, a process compatible with industrial scale for depositing seed layers by flexographic printing is proposed, allowing seed layers to be deposited and patterned swiftly and efficiently in a single step on flexible indium tin oxide coated polyethylene terephthalate substrates, significantly decreasing the time and cost required to produce pressure sensors. The growth conditions of ZnO nanorods on these substrates were also studied to analyze their influence on the morphological and structural characteristics of the nanostructures. Nanorods with length of (0.27 ± 0.04) μm and density of (296 ± 6) nanorods per μm^2 were obtained in microwave-assisted hydrothermal syntheses carried out at 100 °C for 30 min, with a 1 M zinc acetate seed layer and using an equimolar growth solution of zinc nitrate and hexamethylenetetramine. These conditions were used to produce ZnO-based pressure sensors with two patterns (one square and 16 individual squares). Although the single square sensors displayed a higher average output voltage ((12 ± 5) V for an impact pressure of 150 kPa), their response was considerably more variable than the patterned sensors (with 16 squares), which displayed an average output voltage of (8 ± 2) V under an applied pressure of 150 kPa and sensitivity values of (0.06 ± 0.01) V kPa^{-1}, demonstrating their potential for wearables and portable electronics.

New concepts

This work presents an innovative and versatile technique for producing pressure sensors based on zinc oxide (ZnO) nanostructures. Standing out from the commonly used procedures for growing nanostructures, which require time-consuming or expensive processes for depositing and patterning the seed layer from which these materials grow, this study presents an approach combining these two steps, allowing for a cost- and time-effective alternative to produce pressure sensors. The process comprises the deposition of seed layers on commercial conductive substrates by flexographic printing, followed by the growth of ZnO nanorods by microwave-assisted hydrothermal synthesis. The proposed approach allows sensors to be produced in less than one hour. Furthermore, it is shown that the active layer's patterning significantly influences the sensors' performance. The results presented are valuable as they are a step forward in finding the ZnO pattern that maximizes sensor performance and reproducibility using an approach compatible with large-area manufacturing.

1. Introduction

The interest in smart and wearable electronic devices has grown exponentially in recent years.[1] Wearable pressure sensors, based on triboelectric and piezoelectric materials, have gathered much interest in healthcare and biomedical research since they can be used to monitor motion, heart rate and acceleration.[2,3] These sensors present appealing features, such

[a] CENIMAT|i3N, Department of Materials Science, School of Science and Technology, NOVA University Lisbon and CEMOP/UNINOVA, Caparica, Portugal.
E-mail: e.carlos@fct.unl.pt, pmcb@fct.unl.pt

[b] LIBPhys (Laboratory for Instrumentation, Biomedical Engineering and Radiation Physics), NOVA School of Science and Technology, Campus de Caparica, 2829-516, Portugal

† Electronic supplementary information (ESI) available. See DOI: https://doi.org/10.1039/d4mh01000k

as simple and cost-effective production processes, and they allow for easy signal acquisition.[3]

The active layer of pressure sensors can include triboelectric and/or piezoelectric materials. Regarding piezoelectricity, several materials present this property, including inorganics such as aluminum nitride (AlN), barium titanate ($BaTiO_3$), zirconate titanate and zinc oxide (ZnO) or polymeric materials such as polyvinylidene fluoride (PVDF) and polyvinylidene fluoride–trifluoroethylene (P(VDF–TrFE)).[4] Among the most used inorganic piezoelectric materials are lead zirconate titanate (PZT) and ZnO.[5] From these two, ZnO is a non-toxic, biodegradable and biocompatible material, making it an interesting choice to integrate into wearable sensors.[2,6,7] Moreover, this metal oxide is highly abundant in nature.[4,6,8] ZnO has a wide band gap energy of approximately 3.37 eV, large exciton binding energy of 60 meV and a piezoelectric constant (d_{33}) of 9 ± 2 pm V^{-1},[6,7,9] which jointly with this metal oxide's high thermal, chemical and mechanical stability at room temperature[4,6] contribute to its unique optical, electrical and mechanical properties.[5,10] These properties have led to the use of ZnO structures in a myriad of applications, such as in photodetectors, solar cells and nanogenerators applied in sweat, mechanical or touch sensing.[11–15]

Concerning its crystalline structure, ZnO has three polymorphs: cubic zinc blende, cubic rock salt and hexagonal wurtzite.[6,10] At ambient conditions, this metal oxide crystallizes into a hexagonal-packed wurtzite structure composed of alternating planes of zinc cations and oxygen anions along the *c*-axis.[6,10] The non-centrosymmetric property of this structure is originated from the tetrahedral arrangement where four zinc cations surround oxygen anions (and *vice-versa*) present in ZnO crystals.[4] The non-centrosymmetry gives rise to the metal oxide semiconducting and piezoelectric properties used in applications such as pressure sensing.[3] Regarding ZnO piezoelectric properties, they rely on the displacement of dipoles in ZnO crystals. Briefly, no net polarization exists in the rest state as the positive and negative dipoles are aligned at the center of each tetrahedron. When pressure is applied along the *c*-axis, the dipoles' position changes, generating polarization, which is the basis of the ZnO piezoelectricity.[4] This property has been vastly explored in several areas such as in the field of electronics.[4–7]

In flexible electronics, a major milestone is the definition of the substrate and the development of strategies to grow ZnO on this material. The structural properties of the substrate surface strongly influence the growth of aligned ZnO structures.[16,17] The lattice mismatch between the ZnO layer and the substrate can be decreased by either using a single crystalline substrate with a heteroepitaxial ZnO layer or depositing a ZnO seed layer. Being the latter the utmost cost-effective alternative, it is the most explored.[16,17]

ZnO seed layers can be deposited by different techniques, either vapor- or solution-phase approaches, including thermal evaporation, sputtering, atomic layer deposition and pulsed laser deposition or sol–gel and electrochemical deposition, respectively.[4,18–20] Although uniform ZnO layers are produced using these techniques, they require mechanical masks or subtractive processes for patterning the metal oxide layer.[21,22] As such, there is a demand for an approach that can simultaneously deposit and pattern a ZnO seed layer without increasing the complexity of the process. In this scope, printing techniques are an interesting approach as besides allowing the simultaneous deposition and patterning of an ink in a thin film form without extra steps, these additive techniques also offer high reproducibility, scalability and reduction of waste.[23,24] Flexographic printing stands out from the contact printing processes (such as gravure, screen and reverse offset) as this method uses low-cost stamps and allows to reach high printing speed and high yield.[23] This printing approach uses a roller with pattern areas as surface reliefs protruding above non-pattern areas to deposit the material on the substrate.[24]

An essential component of the printing process is the ink, which is used to produce a functional layer.[24] Regarding metal oxide layers, they can be processed using either nanoparticle dispersions or sol–gel solutions.[25] The sol–gel approach is often used to synthesize metal oxide in several forms, including thin films.[10] This method is widely used as it is cost-effective and produces homogeneous layers at relatively low processing conditions.[7,10] The precursor solutions used in sol–gel approaches are generally based on metal salts such as nitrates, acetates or chlorides.[25,26] These mixtures also include a solvent and a stabilizer, also called additive.[7] The most used additives in producing ZnO by sol–gel approaches are monoethanolamine and diethanolamine, which allow the production of stable zinc-based homogeneous solutions by avoiding the precipitation of zinc hydroxide.[7] The deposition of the sol–gel solution on the substrate is typically followed by an annealing step on a hotplate to remove organic residues,[27] improve crystal quality and reduce defects.[28] After the annealing step, a ZnO seed layer is formed, which facilitates the growth of nanostructures by decreasing the thermodynamic barrier to crystallization.[18,29]

ZnO nanostructures can be fabricated through a variety of cost-effective approaches.[4,6] The synthesis method directly influences the properties of the resulting nanostructures, namely crystallinity, alignment, physical and chemical behaviors, morphology and the majority of charge carriers.[4,6,10] Synthesis methods include sol–gel, chemical vapor deposition, hydrothermal synthesis, electrochemical deposition, processes involving emulsion and micro-emulsion environments and controlled precipitation.[3,4,6] Among these, hydrothermal synthesis has been widely explored. For the hydrothermal growth of ZnO nanostructures, a zinc precursor is usually dissolved in water, and another species, such as a hydroxide, is added to tune the growth solution's pH.[4] The syntheses are typically performed at temperatures between the solvent boiling point up to 300 °C and involve the formation of crystal nuclei followed by their growth.[6] The resulting particles are pure ZnO and thus do not require post-treatment.[6] Conventional hydrothermal synthesis routes rely on the conductive and convective mechanisms that lead to a low heating rate and consequently increase the synthesis time. An alternative is a hydrothermal synthesis assisted by microwave irradiation during which the microwaves interact with the molecules in

the growth solution, leading to rapid and uniform heating and consequently to high reaction rates.[30]

Among the several reported ZnO morphologies, one-dimensional (1D) structures stand out from the other shapes. 1D nanostructures such as nanorods, nanotubes and nanowires have been extensively studied as active materials in piezoelectric devices such as mechanical sensors and energy harvesters[3,5,31] as they present increased sensitivity to low-pressure values.[5] These nanostructures present high electron mobility and a high surface-to-volume ratio, which, jointly with the other ZnO properties, can be used to develop high-performance flexible electronics.[3]

In this work, the growth of oriented ZnO nanorods from flexographic printed seed layers by microwave-assisted hydrothermal synthesis and the use of these 1D nanostructures as the active layer of pressure sensors are reported. The seed layer annealing temperature and concentration were optimized to obtain a homogeneous layer. Moreover, the ZnO synthesis conditions, such as zinc precursor type and its ratio regarding the hydroxyl radicals donor, were also varied to determine the conditions yielding high-density nanorod arrays with increased length to maximize the pressure sensors' output signal. The nanorods grown from 1 M seed layers by hydrothermal synthesis at 100 °C for 30 min, where an equimolar zinc nitrate and hexamethylenetetramine solution was used, presented the highest length (0.27 ± 0.04 μm) and density (296 ± 6 nanorods per μm^2) and were used as active layer in pressure sensors. Sensors with two patterns were produced: one square of 4 cm^2 and 16 squares of 0.25 cm^2 spaced by 0.05 μm. The patterned sensors (with 16 squares) displayed an average output voltage of (8 ± 2) V under an applied pressure of 150 kPa and sensitivity values of (0.06 ± 0.01) V kPa^{-1}. The approach used to produce the sensors, namely for the formulation of the seed layer solutions where the greener solvent 1-methoxy-2-propanol was used instead of the commonly used toxic 2-methoxyethanol, was chosen according to the United Nations Sustainable Development Goals and the European Union Green Deal, which dictate the search for sustainable production process. The herein proposed approach allows the production of pressure sensors with sensitivity and output voltage comparable to sensors based on ZnO nanosheets (in a more time-consuming process) already reported in the literature (Table S1, ESI†), thus paving the way for developing high-performance flexible pressure sensors with tunable active layers and compatible with roll-to-roll (R2R) manufacturing.

2. Experimental section

2.1. Precursor solution preparation

A seed layer solution was prepared by first mixing ethanolamine (C$_2$H$_7$NO, Sigma-Aldrich, 99%, CAS: 141-43-5) and 1-methoxy-2-propanol (C$_4$H$_{10}$O$_2$, Carl Roth, ≥99%, CAS: 107-98-2) with magnetic stirring for 5 min. After, zinc acetate dihydrate (Zn(CH$_3$COO)$_2$·2H$_2$O, Alfa Aesar, 98%, CAS: 5970-45-6) was added to the mixture, which was left at 40 °C and 450 rpm

for 1 h to yield a homogeneous solution. The zinc acetate concentration was varied between 0.25 and 1 M and ethanolamine (MEA) was added to 1-methoxy-2-propanol in a molar proportion of 1:1 to zinc acetate dihydrate.

2.2. Seed layer deposition and characterization

The seed layer deposition on indium tin oxide-coated polyethylene terephthalate substrates (PET-ITO, Sigma-Aldrich, surface resistivity of 60 Ω sq^{-1}) was performed by flexographic printing using a RK Flexiproof 100 tabletop printing machine. Before the printing step, the substrates underwent a 15 min ultraviolet (UV)/ozone treatment to improve their wettability using a PSD Pro Heated Series, PSDP-UVT Novascan system; emission wavelengths of 253.7 (90%) and 184.9 nm (10%). Regarding the flexoprinting step, the printing speed was fixed at 50 m min^{-1}, and an anilox roll with a transfer volume of either 13 or 18 cm^3 m^{-2} was used during the printing process, depending on the desired printed area. Two patterns were printed: a square of (20×20) mm^2 and another of 16 squares of (0.5×0.5) mm^2 spaced of 0.5 μm. The (20×20) mm^2 pattern was printed using the higher transfer volume. Different annealing temperatures were tested: 130, 140 and 150 °C. The lab-scale flexographic printing equipment and the stamps used to deposit the seed layers are presented in Fig. S1 (ESI†).

The seed layers and ZnO nanorods grown from them resulting from each condition were studied using scanning electron microscopy (SEM) by using a Hitachi Regulus 8220 scanning electron microscope (Mito, Japan) equipped with an energy-dispersive X-ray spectroscopy (EDS) detector. Before the SEM analysis, the samples were covered with a 20 nm gold/palladium (80/20) layer to improve the images' quality.

The X-ray diffraction (XRD) studies were carried out using a Malvern Panalytical (Almelo, the Netherland) Aeris diffractometer equipped with a PiXcel detector and a monochromatic Cu Kα radiation source with wavelength 1.540598 Å. The crystallinity of the ZnO seed layers and the ZnO nanorods hydrothermally grown from them was analyzed between 10 and 80° (2θ), with a scanning step size of 0.01° and a time per step of 35 seconds.

Atomic force microscopy (AFM) images of the ZnO seed layers were acquired with a Park Systems FX40 equipment (Suwon, South Korea) equipped with AC160TS cantilevers ($f_0 = 300$ kHz; $k = 29$ N m^{-1}) from Olympus Corporation (Tokyo, Japan). The AFM was operated in ambient room conditions and images were acquired in non-contact mode. Images were analyzed in Gwyddion software and exported after low-level flattening. The samples were prepared by fixing PET-ITO substrates with seed layers of 0.25, 0.50 and 1.0 M on AFM stubs with silver glue.

2.3. Hydrothermal growth of ZnO nanorods

Oriented ZnO nanorods were grown from the flexoprinted seed layers by microwave-assisted hydrothermal synthesis. Before the synthesis, the ZnO film underwent a 5 min UV/ozone treatment to improve the nanorods' vertical alignment.[32] This improvement is associated with the changes in the ZnO film

promoted by the surface treatment. Namely, this treatment promotes the decomposition of organic species and the formation of hydroxyl radicals at the surface of ZnO, improving the films' wettability and enabling the hydrothermal growth of a homogeneous layer of ZnO nanorods.[33,34] Moreover, the degradation of organic species leads to the formation of shallow donor levels, which, jointly with changes in the oxygen vacancies caused by the oxygen radicals generated by UV-treating ZnO structures, change the film's carrier concentration.[33,35] These effects of the UV treatment can thus lead to the higher length of hydrothermally grown ZnO nanorods when the seed layer undergoes UV treatment prior to the synthesis.[32,36]

For the synthesis, 25 mL of an aqueous solution of a zinc precursor and hexamethylenetetramine (HMTA, $(C_6H_{12}N_4)_2$, 99%, Sigma-Aldrich, CAS: 100-97-0) was transferred to a 35 mL Pyrex vessel and the PET-ITO substrates were placed at an angle against the inside vessel wall with the seed layer facing down. The hydrothermal synthesis was carried out at 100 °C for 30 min under a power of 100 W using a Discover SP Microwave Reaction System from CEM (North Carolina, USA), according to previous studies.[36] After each synthesis, the substrates were cleaned with deionized water and dried with nitrogen. Different synthesis conditions were tested to study their influence on the nanostructures' length, diameter and density. Namely, nanorod arrays were grown from seed layers with different zinc acetate concentrations (0.25, 0.50 and 1.0 M) using an equimolar (25 mM) growth solution of zinc nitrate hexahydrate and HMTA.[36] Additionally, ZnO nanostructures were produced from 1 M seed layers using growth solution of 25 mM HMTA and either 16 mM zinc acetate dihydrate, 25 mM zinc nitrate hexahydrate $(Zn(NO_3)_2 \cdot 6H_2O$, Sigma-Aldrich, 98%, CAS: 10196-18-6) or 39 mM zinc chloride $(ZnCl_2$, Merck, ACS, CAS: 7646-85-7) according to procedures reported in the literature.[37] As the synthesis with zinc nitrate produced high-density nanorod arrays with improved length, it was used to assess the influence of the ratio between zinc and HMTA on the nanostructures' properties. In this scope, the features of nanorods grown from 1 M seed layers and nutrient solutions whose zinc:HMTA molar ratio was 1:1, 1:2 and 2:1 were also evaluated.

The nanorod arrays' features, namely length, diameter and density, were studied using ImageJ software and SEM images. The average particle length and diameter (and corresponding standard deviation) were calculated from the dimensions of 50 nanoparticles. ImageJ software was also used to enhance the features of the SEM images to identify the nanorods and estimate their density more accurately. First, the images' contrast was increased, and the detail was accentuated using the "Sharpen" function, followed by another contrast adjustment, where the number of pixels in the image allowed to become saturated corresponded to 20% and the normalization and histogram equalization were performed. Next, a bandpass filter from 0 to 30 was applied to the adjusted images, and then the image thresholds were adjusted to include the range 165 to 255. The number of nanorods was estimated using the "Analyze Particles" function, in which the circularity was restricted to the

range 0 to 0.7. The number of particles was divided by the image area to obtain the local density of nanostructures. The presented values are the average density obtained in 5 regions with dimensions of (2.54×1.90) μm^2.

2.4. ZnO-based pressure sensor fabrication and characterization

ZnO nanorods were grown on PET-ITO substrates from 1 M seed layers by microwave-assisted hydrothermal synthesis for 30 min at 100 °C. An equimolar (25 and 50 mM) aqueous mixture of zinc nitrate hexahydrate and HMTA was used as a growth solution, as these conditions yielded nanorods with increased length and density.

After the growth of the ZnO nanorods from the flexoprinted seed layer, a poly(methyl methacrylate) (PMMA, Sigma-Aldrich, $M_w \sim 996.000$, CAS: 9011-14-7) layer was deposited on top of the nanostructures by spin-coating. The polymer was mixed with acetone (Sigma-Aldrich, $\geq$99.5%, CAS: 67-64-1) by magnetic stirring for 1 h at 400 rpm to produce a homogeneous transparent 10 wt% PMMA solution. This solution was deposited on top of the nanostructures by spin-coating at 4000 rpm for 15 s with an acceleration of 4000 rpm. The samples were dried at room temperature, after which PET-ITO electrodes were placed on top of the ZnO nanostructured films. The characterization of the produced sensors was performed by applying a mechanical stimulus in a contact area of 4 cm^2 with a force between 30 and 60 N at a frequency of 2 Hz with a homemade machine. A 50 MHz bandwidth oscilloscope (Tektronix, TDS 2001C) was used to measure the voltage generated by the sensors. The ZnO nanostructure-based pressure sensor production process is illustrated in Fig. 1.

3. Results and discussion

3.1. Characterization of the ZnO nanorod arrays

The presence of ZnO seed layers has been reported to lead to a higher ZnO density.[2] The properties of these layers, such as crystalline type, purity, doping uniformity, surface morphology and contact interface, strongly influence device performance in electronic devices.[24] As so, a first study was conducted on the influence of the seed layer annealing temperature on the morphological features of hydrothermally grown ZnO nanorods. This study was fundamental for developing high-performance pressure sensors as the ink-drying process is essential for the printed pattern to acquire specific electronic properties.[24] A zinc acetate solution with a 1 M concentration was deposited on PET-ITO substrates and the subsequent annealing was performed at temperatures between 130 and 150 °C for 10 min. A zinc acetate precursor was used because it improves the vertical alignment of ZnO nanorods.[38] The morphology of the seed layers deposited via flexographic printing and the nanorod arrays are presented in Fig. 2. It is worth noting that the study of the influence of the annealing temperature and the other analysis presented in this section were performed with patterns of 16 squares of (0.5×0.5) mm^2.
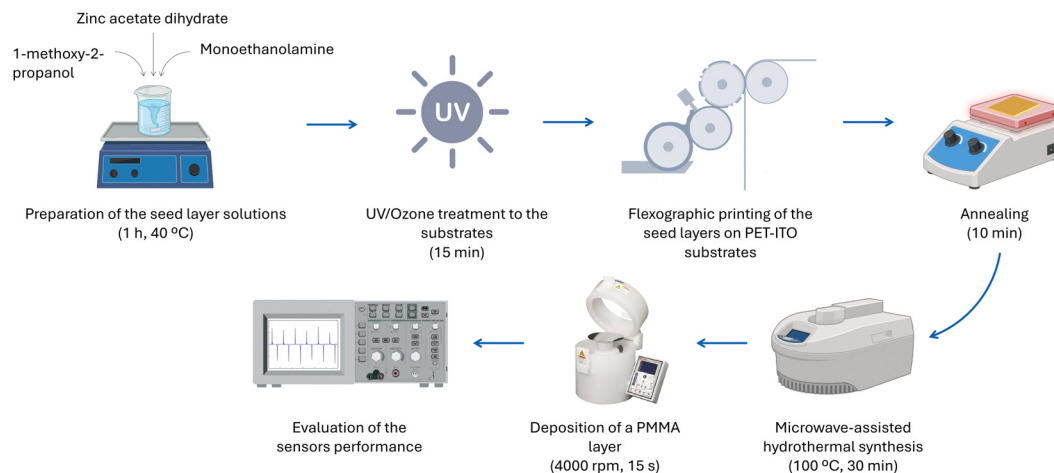
Fig. 1 Diagram illustrating the production process and characterization of the developed pressure sensors based on oriented ZnO nanostructures.
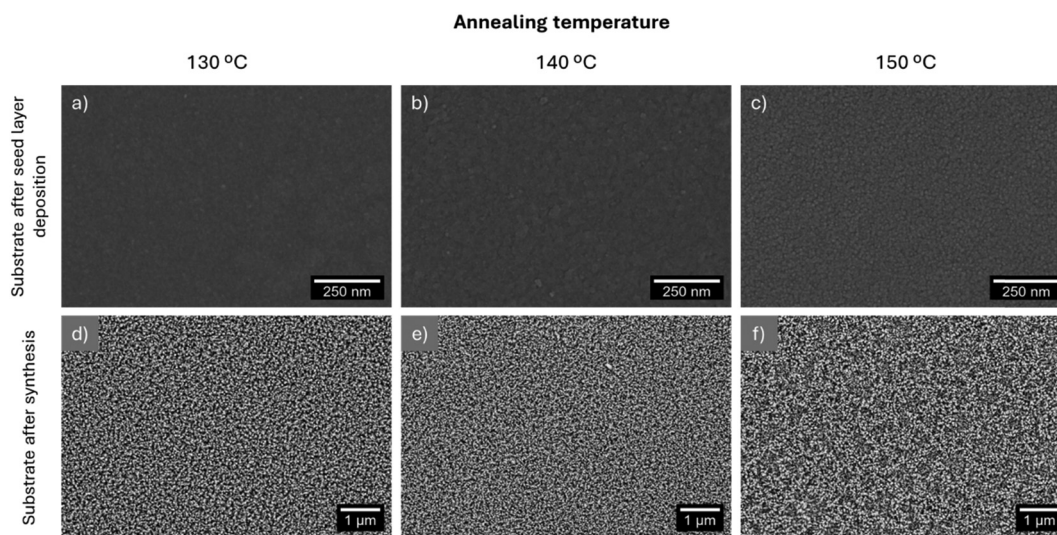

Fig. 2 Morphology of the flexographic printed seed layer and the ZnO nanorods grown from layers annealed at 130 (a) and (d), 140 (b) and (e) and 150 °C (c) and (f).

The liquid species in the seed layer solution, namely 1-methoxy-2-propanol and MEA have boiling points of 120 °C and 170 °C, respectively. As so, annealing should be carried out at a minimum temperature of 170 °C to ensure the complete removal of the organic solvents and the formation of a crystalline and continuous ZnO seed layer.[39] However, the PET-ITO substrates started contracting irregularly after being heated at 150 °C, which is in accordance with the reported lack of dimensional stability of substrates such as polyethylene naphthalate (PEN) and PET when processed at 150–200 °C.[40] This limitation might be associated with PET's cold crystallization temperature being around 150 °C.[41] As so, this was the maximum temperature tested. The minimum annealing temperature was fixed at 130 °C to ensure the complete removal of 1-methoxy-2-propanol. Fig. 2(a)–(c) show that the seed layers present a more granular appearance for higher annealing temperatures, as reported previously.[42] The samples resulting from annealing at 130 and 140 °C

present only minor differences; however, the layer resulting from annealing at 150 °C has a more granular appearance, which influenced the nanorods' growth since the existence of discontinuities in the nanorod arrays shown in Fig. 2(f) is clearly visible.

Higher annealing temperatures have been reported to increase the diameter and length of ZnO nanorods.[42,43] Al-She'irey *et al.* studied the influence of the seed layer annealing temperature on the properties of hydrothermally synthesized nanorods. This seed layer composition included zinc acetate dihydrate, diethanolamine and ethanol and the annealing temperature was varied between 300 and 500 °C. The diameter and length of hydrothermally synthesized ZnO nanorods increased with increasing seed layer annealing temperature.[42,43] Higher seed layer annealing temperature leads to the coalescence of nuclei at the seed layer's grain boundaries, leading to an increase in the nanorods' diameter.[43,44] On the other hand, the

Concentration of zinc precursor in the seed layer solution
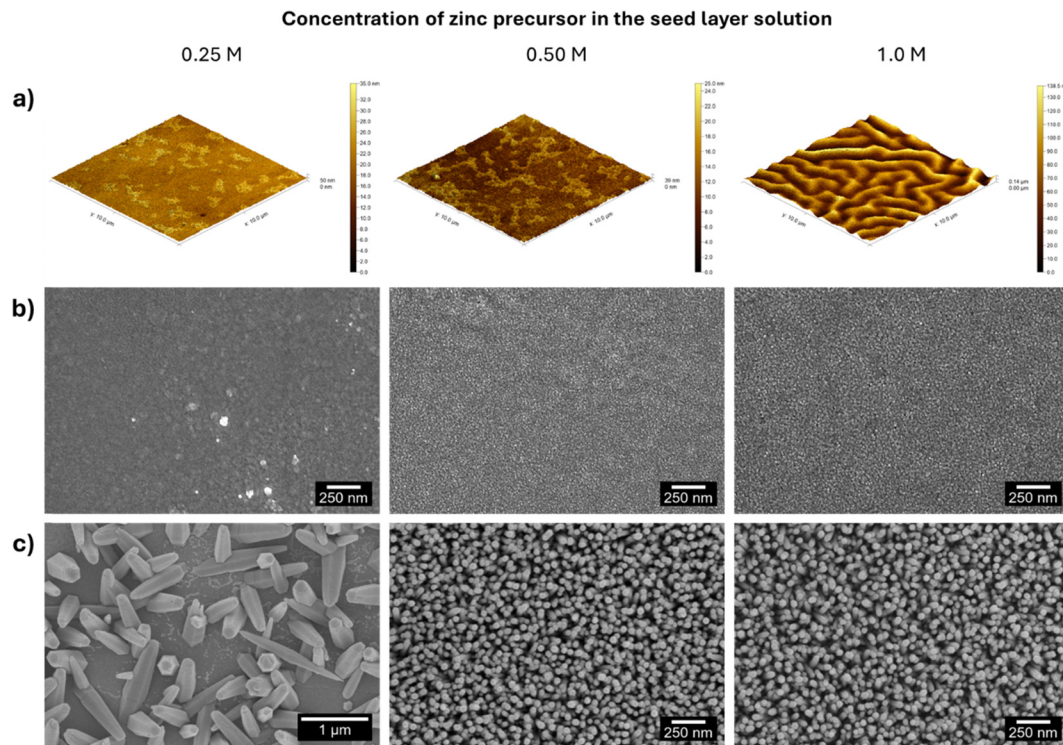
Fig. 3   (a) AFM and (b) SEM images of the seed layers printed on PET-ITO substrates with 0.25, 0.50 and 1.0 M zinc acetate precursor solutions. (c) Morphology of the nanostructures hydrothermally grown from each seed layer.

increase in nanorods' length is associated with the preferential growth of ZnO particles (which possess a wurtzite structure) along the c-axis.[42,44] In line with these results, the seed layer annealing temperature was fixed at 140 °C.

Next, the influence of zinc concentration in the seed layer solution on the properties of the printed films was studied. In this scope, zinc acetate solutions with 0.25, 0.50 and 1 M concentrations were deposited on commercial PET-ITO substrates and annealed at 140 °C for 10 min. The surface roughness of the seed layers was studied with AFM (area = 100 μm^2), and the corresponding 3D images are presented in Fig. 3(a). The 2D images are presented in Fig. S2 (ESI†).

The AFM images revealed a root mean square roughness of 3.058, 3.553 and 24.07 nm for the seed layers with 0.25, 0.50 and 1 M zinc acetate, respectively. It is worth noting that this trend is in accordance with previous studies where increasing zinc acetate concentration led to an increase in ZnO thin films' roughness.[45] The seed layers were further studied using SEM, and the corresponding images are presented in Fig. 3(b). A comparative analysis of the images reveals an increase in the dimensions of the seed layer particles due to their coalescence caused by an increase in the precursor concentration.

SEM images of non-patterned seed layers deposited on PET-ITO substrates using 0.25, 0.50 and 1.0 M zinc acetate solutions are presented in Fig. S3 (ESI†). A comparison of the morphological features of non-patterned and patterned seed layers underlines their similarity, demonstrating that the patterning process does not alter the topology of the layers deposited by flexographic printing, from which the nanorods grow.

ZnO nanorods were grown from seed layers by microwave-assisted hydrothermal synthesis and SEM images of the obtained nanostructures (Fig. 3(c)) were used to calculate the nanorods' length, diameter and density. The estimated values are presented in Table S2 (ESI†) and Fig. 6(a). The analysis of the nanorod arrays' features leads to the conclusion that although the 0.25 M seed layer produces nanorods with higher length, the nanostructures' density is relatively low, which may be associated with the particle agglomerates present in the seed layer seen in Fig. 3(b). Concerning the nanorods grown from 0.50 and 1 M seed layers, the nanostructure arrays have a similar density. However, the length of the nanorods is superior when the concentration of zinc precursor in the seed layer is higher, a trend observed in another work.[39] The higher length of the synthesized nanorods can be ascribed to the more uniform particle size and high compactness of the seed layer.[39]

Similarly to the results presented in this work, a proportional relation between the nanorods' length and the seed layer concentration has been previously reported.[39] The concentration of the seed layer deposited on fluorine-doped tin oxide-coated glass substrates was varied between 0.05 and 0.5 M and the sample resulting from the highest seed layer concentration yielded nanorods with increased length. Increasing the seed layer concentration (up to 0.3 M) led to the best vertical alignment and increased density, which was ascribed to the homogeneity of the films in terms of particle and grain sizes.

The proportional relation between the nanorods' aspect ratio, which is the ratio between the length and the diameter of 1D nanostructures, and the pressure sensor output voltage

was verified in previous works, *i.e.*, sensors based on more extended structures (up to 3 μm long) yielded higher voltage amplitudes.[46,47] These results derive from the higher deformation degree of these nanostructures, which enhances the displacement of the charge centers present in ZnO along the *c*-axis.[48] As so, 1 M seed layers were chosen as the optimal condition as they generated longer 1D ZnO structures, which was reported to lead to better piezoelectric performance.[46] A cross-sectional SEM image of this seed layer is presented in (Fig. S4a, ESI†), where a homogeneous cover of the PET-ITO substrate is visible. ZnO nanorods grown from this film are also shown in Fig. S4b (ESI†), where the growth of these nanostructures can be discerned from the layer deposited by flexographic printing. The particles in this layer act as nucleation sites, decreasing the thermodynamic barrier to crystallization and favoring the vertical growth of 1D nanostructures.[18,29]

Regarding the crystallographic structure of the seed layers and the produced nanorods, the crystallinity of the seed layers was primarily evaluated using XRD (Fig. S5b and c, ESI†). However, no peaks were detected, which could be owing to the very intense peak around 25.0°, characteristic of the PET-ITO substrate (Fig. S5a, ESI†) masking the seed layer's peaks or due to the amorphous nature of this layer.[1] It is worth mentioning that no ITO-related peaks were observed in the PET-ITO substrate's XRD pattern underlying the ITO film's amorphous nature.[1] ZnO nanorods were grown from the seed layers with different concentrations and the diffractograms are presented in Fig. 4(a).

The diffractograms displayed in Fig. 4(a) present a peak at around 34.5° which corresponds to the (002) diffraction peak characteristic of ZnO hexagonal wurtzite structure (ICDD card 36-1451), which can be attributed to the preferential growth of the ZnO nanorods along the direction of the *c*-axis.[2,3,5] When zooming in on the region between 30 and 40°, where the typical ZnO peaks are present (Fig. 4(b)), diffraction peaks at 31.7 and 36.2° are detected. These peaks can be attributed to the (100) and (101) ZnO crystal planes. Moreover, the pattern of ZnO nanorods grown from a 1 M seed layer presents the most intense (002) diffraction peak, indicating that seed layer formulation also impacts the crystallinity of the resulting nanostructures.[24] These results reinforce the choice of 1 M

seed layers to proceed with the studies as this layer led to nanostructures with high density and length and improved crystallinity, desirable features in pressure sensors.

The precursors used to grow ZnO nanostructures on different substrates by hydrothermal synthesis have a vital role as varying their type or concentration alters the nanostructures' properties.[29] In particular, anion regulation has been proposed to tune the morphology of hierarchical ZnO arrays.[37] In line with these results, ZnO nanorods were grown from 1 M seed layers, annealed at 140 °C for 10 min, using different zinc precursors, namely zinc acetate dihydrate, zinc chloride and zinc nitrate and the results are presented in Fig. 5. The nanorods' average length, diameter and density are present in Fig. 6(b) and listed in Table S2 (ESI†).

An initial analysis of the nanorod images in Fig. 5 reveals several morphological differences between the nanostructures produced with different zinc precursors, in line with previous reports describing counter-ions role as capping agents.[49] Counter-ions influence the formation and stability of zinc-based intermediate species and consequently, of the obtained ZnO particles.[49] The rods resulting from synthesis with acetate have pencil-like tips, while the nanostructures produced with zinc nitrate have flat tops similar to the nanostructures produced with zinc chloride. However, nanoplates can be detected among the nanorod arrays synthesized using zinc chloride, which can be attributed to the preferential attachment of chloride anions to the (002) plane of the ZnO wurtzite structure, hindering the growth along this direction and leading to the formation of nanoplates.[50] Comparing the nanorods resulting from the various synthesis conditions, the nanostructures produced with zinc acetate dihydrate present the highest length among the produced samples, as evidenced in Fig. 6(b). However, the highest nanorod density was obtained in the synthesis with nitrate. Therefore, the following tests were carried out with nanorods produced with zinc nitrate since a higher density of nanostructures will, in principle, result in pressure sensors with improved performance.

A zinc precursor and a source of hydroxyl radicals are vital for the hydrothermal synthesis of ZnO nanostructures. HMTA has been vastly used as a complexing agent and provider of hydroxyl radicals.[51,52] This chemical species is also used as
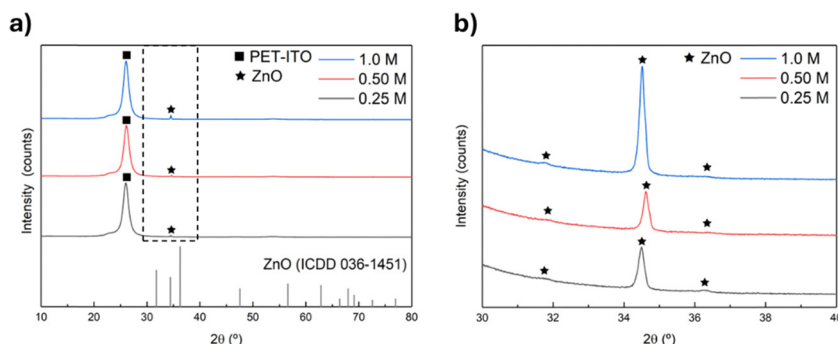

Fig. 4 XRD patterns of the (a) ZnO nanorods grown from seed layers with 0.25, 0.50 and 1.0 M precursor concentrations (2θ between 10 and 80°). (b) Zoom of the ZnO nanorods' XRD patterns in the region between 30 and 40° (2θ).
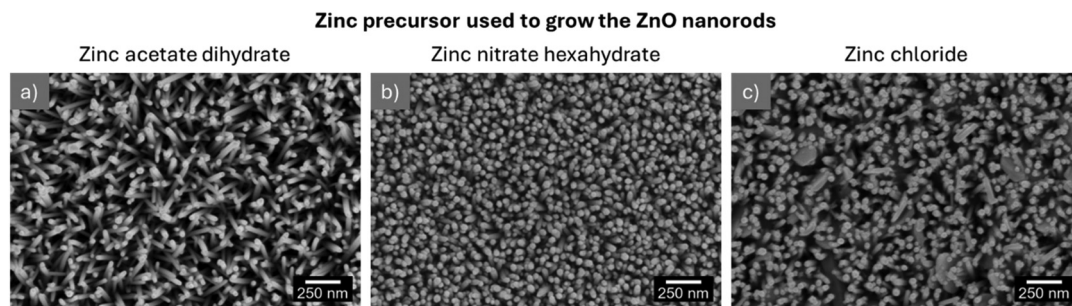
Zinc precursor used to grow the ZnO nanorods

Fig. 5 SEM images of ZnO nanorods grown from 1 M seed layers using (a) zinc acetate dihydrate, (b) zinc nitrate hexahydrate and (c) zinc chloride.
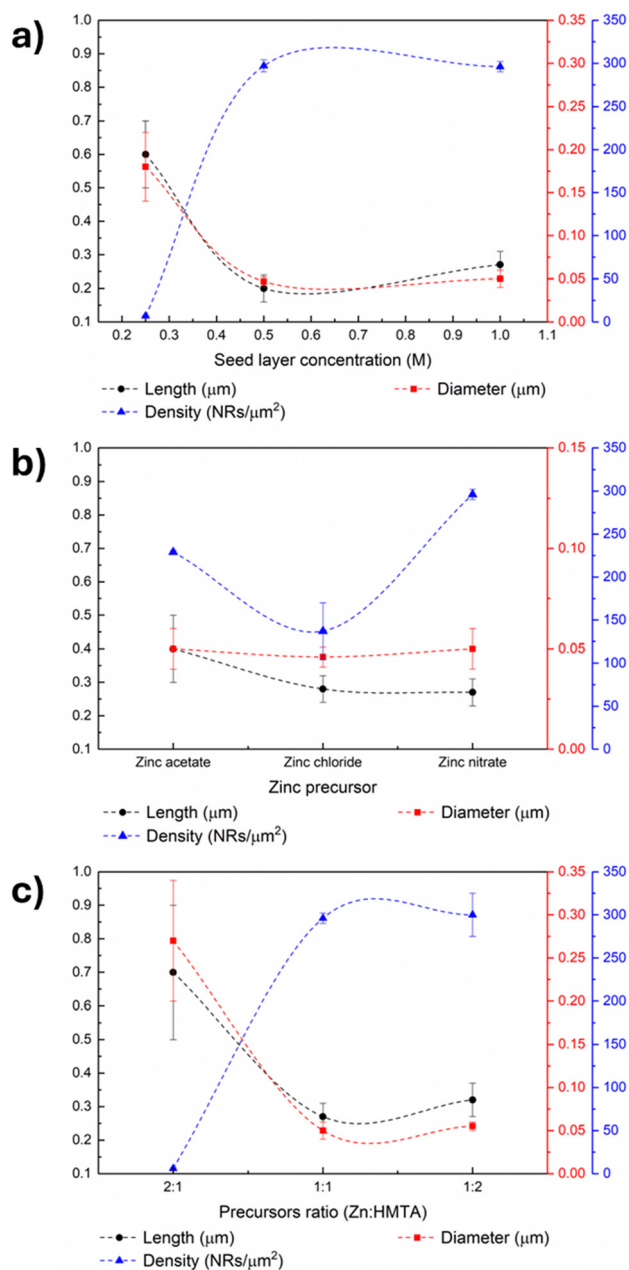

Fig. 6 Length, diameter and density of ZnO nanorods grown: (a) from seed layers with different zinc acetate concentrations, (b) using synthesis solutions with different zinc precursors and (c) using different zinc : HMTA ratios.

a structure-directing agent since it preferentially attaches to the lateral nonpolar facets of ZnO crystals, thus promoting the nanostructures' growth along the *c*-axis since radial growth is hindered.[18,53] In this scope, the role of HMTA in the hydrothermal growth of ZnO nanorods from 1 M seed layers was evaluated by performing different syntheses where the molar ratio between zinc nitrate hexahydrate and HMTA was varied. Three synthesis conditions were tested, namely, syntheses were carried out in which the molar concentration of HMTA was double, and half of the zinc nitrate concentration and the third was performed under equimolar conditions. The SEM images are presented in Fig. S6 (ESI†), and the estimated nanorod length, diameter and density are presented in Fig. 6(c) and Table S2 (ESI†).

The role of HMTA as a structure-directing agent of ZnO nanorods has been stated in several reports.[18,54] The HMTA molecules selectively bind to the nonpolar crystal planes of zincite crystals, creating a steric hindrance effect and thus promoting axial growth along the *c*-axis.[55] Namely, nanorods synthesized using solutions with zinc nitrate hexahydrate and HMTA in different ratios exhibited increased length and reduced diameter when HMTA concentration was higher than that of the zinc precursor.[18] The trend observed in this work is partially in accordance with these results, as synthesis carried out using excess HMTA in relation to zinc precursor led to the formation of nanostructures with a higher length of (0.32 ± 0.05) μm and reduced diameter compared to the particles obtained using equimolar growth solutions, which presented a length of (0.27 ± 0.04) μm. However, the samples produced using the lowest HMTA concentration presented the highest length $((0.7 \pm 0.2)$ μm). Nonetheless, the nanostructures in this sample differ significantly from the other two, indicating that a Zn : HMTA ratio of 2 is a limiting condition for forming oriented ZnO nanorod arrays. Regarding density, the results show that when the zinc concentration is higher than that of HMTA, the nanorod density is very low (6 nanorods per μm^2). These results suggest that the growth of these structures is only promoted when the zinc concentration is at least equal to that of HMTA. When comparing equimolar conditions and those with excess HMTA, a higher concentration of the latter results in the growth of longer nanostructures, as expected. However, the samples resulting from this condition present more significant variability in terms of density. Therefore, as

the difference in nanorod size is not considered significant, the equimolar condition was defined as optimal for obtaining samples with a high density of nanostructures of acceptable length.

To summarize, the protocol for growing nanostructures on PET-ITO substrates to develop pressure sensors was based on the conditions that yielded samples with a high density of nanostructures throughout the sample and maximized their length. This protocol consists of depositing a seed layer by flexographic printing using a 1 M zinc acetate solution dissolved in 1-methoxy-2-propanol, followed by annealing at 140 °C for 10 min. Then, after a 5-minute UV/ozone treatment of the resulting film, ZnO nanostructures are grown by microwave-assisted hydrothermal synthesis using an equimolar zinc nitrate hexahydrate and HMTA solution. The synthesis temperature and time are 100 °C and 30 min, respectively. After the nanorods' growth, a layer of PMMA is deposited on top of these nanostructures as PMMA is a polymer widely used to optimize the performance of piezoelectric devices.[4] After the PMMA deposition, the top electrode is positioned over the ZnO nanorod arrays. Sensors with two distinct patterns were produced, and their response was evaluated for impact forces between 30 and 60 N.

3.2. Flexographic printed microwave-assisted hydrothermally grown ZnO pressure sensors

Regarding the functioning of ZnO pressure sensors, it relies on the deformation of the ZnO nanostructures.[8] Therefore, a second PET-ITO electrode was positioned on top of aligned ZnO nanorods grown on PET-ITO substrates (Fig. 7(a)) and the assembly was subjected to impact pressures between 75 and 150 kPa, as its active area is equal to 4 cm^2 and the corresponding voltage response was evaluated.

The application of an external force causes the deformation of the ZnO nanostructures along the *c*-axis and the misalignment of positive and negative dipoles present in ZnO, leading to polarization in the ZnO crystal. This polarization causes the electrons to flow across an external circuit and to accumulate on the bottom electrode. Upon the end of application of the external force, the electrons flow in the opposite direction.[5,8] When a polymer surrounds the ZnO nanostructures, the polarization is enhanced due to the presence of a triboelectric electric field. Additionally, the interfacial polarization near the interface ZnO/polymer improves surface charge density and consequently enhances the sensor's performance.[8] The phenomenon of charge migration can be seen in Fig. 7(b), where the positive and negative peaks indicate charge flowing in opposing directions. The magnitude of the positive and negative peaks is slightly different, which can be attributed to the difference in strain rate during the compression and releasing cycles.[5]

Sensors based on ZnO nanorods grown from seed layers with a pattern of a single square of 4 cm^2 using a 50 mM growth solution were tested under different impact pressures, and the peak-to-peak voltage values are presented in Fig. 7(c). It is worth noting that sensors were also produced using a 25 mM growth solution. However, these sensors did not present an output voltage proportional to deformation and the devices also presented poor reproducibility (Fig. S7, ESI†), which was attributed to the short length of the ZnO nanorods grown on the PET-ITO substrates derived from the low concentration of the growth solution, as the nanostructures' length increases proportionally with the solution concentration.[56] In turn, the sensors presented in Fig. 7(c) exhibit the expected proportional trend between peak-to-peak voltage and impact pressure, hence 50 mM was the concentration chosen to carry out the microwave-assisted hydrothermal growth of ZnO nanorods. It should be noted that there are some differences in the peak-to-peak voltage of different sensors, which may be due to variations in nanorod growth associated with the solution process used for their production.

The response of piezoelectric devices has been reported to decrease due to the screening effect of free charges.[4,5] The cause of this effect can be either internal or external.[4] The source of the internal screening effect is either the excess of free electrons, as ZnO is an n-type semiconductor or donor crystal defects. Upon generation of a piezo-potential, free electrons migrate towards the positive region of the created electric field, causing a reduction or even neutralization of the generated piezo-potential.[4,57] External screening results from inadequate electrode materials, which leads to leakage of charges *via* the metal–semiconductor interface (when an external load is applied) and suppression of the piezoelectric effect due to inappropriate energy barriers between the ZnO nanostructures and the electrode.[4] Patterning ZnO nanostructures grown on a PET-ITO substrate can reduce the internal screening effect as it separates the sensor's active area in different independent units, hindering the free charge carriers present in certain nanostructures (that experience less strain) from decreasing the generated piezo-potential.[58] Based on these studies, sensors with the same area as the ones presented in Fig. 7(c) but based on a pattern of 16 squares spaced by 0.5 μm were tested under the same impact pressures and the results are presented in Fig. 7(d).

The results presented in Fig. 7(c) and (d) indicate a proportional relation between the impact pressure and the peak-to-peak output voltage, as expected. A higher impact pressure causes a more considerable deformation of ZnO nanostructures besides promoting a higher contact between the active layer and the electrodes, which leads to higher output signals.[8] The output voltage of single square sensors is higher; however, comparing the two types of sensors' performance is complex as other features should be considered besides the output voltage. Namely, the response of patterned sensors is less variable between sensors. These results clearly demonstrate the influence of ZnO active layer patterning on the performance of pressure sensors. A video depicting the sensor's functioning is included as ESI.†

The slope of the output voltage response to applied pressure was used to estimate the sensitivity of the produced pressure sensors.[5] The sensitivity values obtained for each sensor are presented in Table S3 (ESI†) and Fig. 8, where single square and patterned sensors represent the sensitivity values of sensors
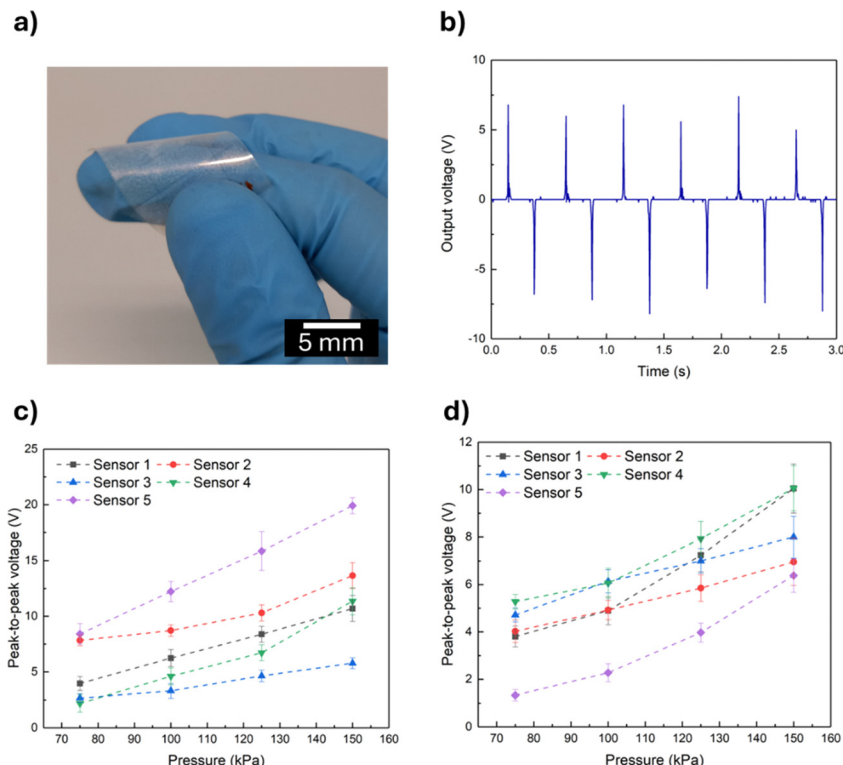
Fig. 7 (a) Optical image of the ZnO nanorods grown from a patterned seed layer. (b) Output voltage of single square pressure sensors for an impact pressure of 100 kPa. Peak-to-peak voltage of sensors based on (c) one square of 4 cm^2 and (d) 16 squares of 0.25 cm^2 of aligned ZnO nanorods.
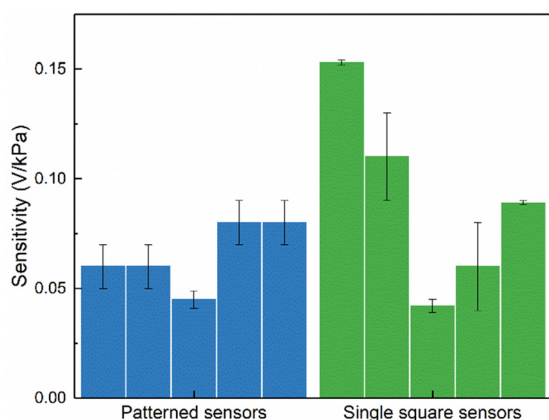

Fig. 8 Sensitivity values of non-patterned (single square) and patterned pressure sensors. Each bar represents the sensitivity of a different sensor.

based on seed layers composed of one square and 16 squares, respectively.

Analysis of the data in Table S3 (ESI†) shows that some regressions have a lower R^2, which may be associated with the lower linearity of certain sensors in the low-pressure region. This behavior may derive from slight variations in the nanorod size between samples. Furthermore, when comparing the sensitivity values of the two sensor types presented in Fig. 8, it can be seen that the values obtained for the patterned sensors exhibit less variability than those obtained for the single square

sensors. This trend indicates that patterning the ZnO active layer hinders the screening effect and ensures good reproducibility and sensor performance.

The output voltage of the pressure sensor based on nanorods grown from a patterned seed layer and presented in Fig. 7(d) as "Sensor 4" was measured over 5000 cycles of impact at 150 kPa in order to evaluate the device stability over time. The results are presented in Fig. S8 (ESI†). The device shows negligible output voltage variations during the initial 1000 cycles. However, a slight reduction in the sensor's output voltage is detected after 5000 cycles (less than 1 V). Increasing the thickness of the PMMA layer or including other polymers in the sensor's architecture could increase its durability.

Regarding the ZnO-based pressure sensors' long-term stability, "Sensor 4" was tested 2 months after being stored in ambient conditions and showed a peak-to-peak voltage of (10.5 ± 0.1) V, a value similar to the initial tests in which voltages of (10.1 ± 0.9) V were obtained. These results highlight the long-term stability of the developed sensors and demonstrate that these devices do not require special storage conditions to maintain a good performance.

Table S1 (ESI†) summarizes key points regarding the production and performance of some pressure sensors based on ZnO nanostructures reported in the literature. Comparing the performance of the sensors developed in this work with that of devices reported in the literature is difficult due to the wide range of protocols used to characterize ZnO-based pressure sensors. However, when analyzing Table S1 (ESI†), it is clear

that devices produced by processes such as chemical vapor deposition exhibit excellent performance, reaching sensitivity values of 0.18 V kPa^{-1}, since these processes enable the growth of high-length nanostructures with improved alignment.[3] However, vapor-phase processes are time- and energy-consuming and incompatible with some substrate materials. Regarding the herein-developed flexographic printed sensors, these devices have a sensitivity of (0.06 ± 0.01) V kPa^{-1}, which is comparable to that of sensors based on ZnO nanosheets (sensitivity = 0.0318 V kPa^{-1}) produced by hydrothermal synthesis in a much longer process than the one proposed in this work.[5] Thus, it is clear that the response of the proposed sensors has room for improvement, namely by introducing polymers that improve the sensors' output, *i.e.*, the output signal of ZnO-based sensors increased from 37.50 V to 121.3 V when polytetrafluoroethylene (PTFE) was incorporated in the devices' architecture.[8,59] However, the proposed procedure for producing pressure sensors stands out from those reported in the literature since by combining printing techniques with microwave-assisted hydrothermal growth it allows sensors to be produced much more swiftly (within 1 hour) and enables them to be patterned without resorting to techniques such as photolithography, in an approach compatible with R2R manufacturing.[60]

4. Conclusions

A new method was proposed to produce printed ZnO-based pressure sensors by first depositing a seed layer on indium tin oxide-coated polyethylene terephthalate substrates by flexographic printing and then growing ZnO nanorods from this layer by microwave-assisted hydrothermal synthesis. The influence of the seed layer annealing temperature and concentration, zinc precursor present in the growth solution and the molar ratio between the zinc precursor and the commonly used hydroxyl radicals donor hexamethylenetetramine (HMTA) were studied. The highest values of nanorod length and density were (0.27 ± 0.04) µm and (296 ± 6) nanorods per µm^2, respectively. These nanostructures were grown from 1 M seed layers using zinc nitrate and HMTA equimolar growth solutions. Synthesis time and temperature were fixed at 30 min and 100 °C. Nanorods were grown from seed layers with different patterns (one square of 4 cm^2 and 16 individual squares of 0.25 cm^2) using these conditions and incorporated into pressure sensors. Patterning the seed layer proved to play an essential role in the sensors' performance since, although the non-patterned sensors present higher output signals (average output signal of (12 ± 5) V for an impact pressure of 150 kPa), the sensors composed of 16 squares present better reproducibility (average output signal of (8 ± 2) V for an impact pressure of 150 kPa) and sensitivity values of (0.06 ± 0.01) V kPa^{-1}. The higher reproducibility is evidenced by the minor standard deviation associated with the average output voltage of the patterned sensors and the reduced dispersion of their sensitivity values compared to the sensitivity of the non-patterned sensors. These observations indicate that patterning the ZnO layer can reduce the screening effect affecting pressure

sensors' piezoelectric response. The promising performance of the devices presented renders the proposed method a fundamental tool for the straightforward and time-effective production of ZnO pressure sensors with easily tailorable architecture and reproducible and stable performance.

Data availability

The data that support the findings of this communication manuscript are available on request from the corresponding author.

Conflicts of interest

The authors declare no conflicts of interest.

References

1 I. Z. Papp, A. Alegría, Z. Kónya and Á. Kukovecz, Investigation into the effect of ZnO nanorod coating on the thermal-mechanical and dielectric properties of ITO coated PET, *Mater. Res. Bull.*, 2022, **149**, 111701.

2 G. Arrabito, A. Delisi, G. Giuliano, G. Prestopino, P. G. Medaglia, V. Ferrara, F. Arcidiacono, M. Scopelliti, D. F. Chillura Martino and B. Pignataro, Self-Cleaning Bending Sensors Based on Semitransparent ZnO Nanostructured Films, *ACS Appl. Eng. Mater.*, 2023, **1**, 1384–1396.

3 M. Kumari, R. K. Prasad, M. K. Singh, P. K. Iyer and D. K. Singh, Piezo-resistive pressure sensor based on CVD-grown ZnO nanowires on Polyethylene Tetrathalate substrate, *arXiv*, 2023, arXiv:2307.13805, DOI: **10.48550/arXiv.2307.13805**.

4 A. T. Le, M. Ahmadipour and S.-Y. Pung, A review on ZnO-based piezoelectric nanogenerators: Synthesis, characterization techniques, performance enhancement and applications, *J. Alloys Compd.*, 2020, **844**, 156172.

5 S. Rafique, A. K. Kasi, Aminullah, J. K. Kasi, M. Bokhari and Z. Shakoor, Fabrication of Br doped ZnO nanosheets

piezoelectric nanogenerator for pressure and position sensing applications, *Curr. Appl. Phys.*, 2021, **21**, 72–79.

6 S. Raha and M. Ahmaruzzaman, ZnO nanostructured materials and their potential applications: progress, challenges and perspectives, *Nanoscale Adv.*, 2022, **4**, 1868–1925.

7 M. Ben Aziza, Y. Litaiem, R. Chtourou and S. Ammar, The Influence of Different Stabilizers on Properties of Sol–Gel Spin-Coated Zinc Oxide Films, *Braz. J. Phys.*, 2021, **51**, 722–730.

8 S. Ippili, V. Jella, J. M. Lee, J.-S. Jung, D.-H. Lee, T.-Y. Yang and S-G. Yoon, ZnO–PTFE-based antimicrobial, anti-reflective display coatings and high-sensitivity touch sensors, *J. Mater. Chem. A*, 2022, **10**, 22067–22079.

9 A. Rovisco, A. dos Santos, T. Cramer, J. Martins, R. Branquinho, H. Águas, B. Fraboni, E. Fortunato, R. Martins, R. Igreja and P. Barquinha, Piezoelectricity Enhancement of Nanogenerators Based on PDMS and ZnSnO₃ Nanowires through Microstructuration, *ACS Appl. Mater. Interfaces*, 2020, **12**, 18421–18430.

10 S. Arya, P. Mahajan, S. Mahajan, A. Khosla, R. Datt, V. Gupta, S.-J. Young and S. K. Oruganti, Review—Influence of Processing Parameters to Control Morphology and Optical Properties of Sol–Gel Synthesized ZnO Nanoparticles, *ECS J. Solid State Sci. Technol.*, 2021, **10**, 023002.

11 H. Wang, P. Zhang and Z. Zang, High performance CsPbBr3 quantum dots photodetectors by using zinc oxide nanorods arrays as an electron-transport layer, *Appl. Phys. Lett.*, 2020, **116**(16), 162103.

12 Z. Zang, Efficiency enhancement of ZnO/Cu₂O solar cells with well oriented and micrometer grain sized Cu₂O films, *Appl. Phys. Lett.*, 2018, **112**(4), 042106.

13 B. Baro, S. Khimhun, U. Das and S. Bayan, ZnO based triboelectric nanogenerator on textile platform for wearable sweat sensing application, *Nano Energy*, 2023, **108**, 108212.

14 S. Jiang, X. Zhao, J. Zhang, B. Fang, H. Chen, L. Ma, Z. Ding, J. Wei and N. Hao, Metal-doped functional zinc oxide nanosheets as flexible piezoelectric generator for self-powered mechanical sensing, *Sens. Actuators, A*, 2024, **371**, 115337.

15 S. I. Petrushenko, M. Fijalkowski, V. R. Kopach, Y. M. Shepotko, K. Adach, S. V. Dukarov, V. M. Sukhov, A. Fedonenko, A. L. Khrypunova and N. P. Klochko, Carbon fabric coated with nanostructured zinc oxide layers for use in triboelectric self-powered touch sensors, *J. Mater. Sci.: Mater. Electron.*, 2024, **35**, 414.

16 E. Chalangar, O. Nur, M. Willander, A. Gustafsson and H. Pettersson, Synthesis of Vertically Aligned ZnO Nanorods Using Sol-gel Seeding and Colloidal Lithography Patterning, *Nanoscale Res. Lett.*, 2021, **16**, 46.

17 N. Basinova, O. Cernohorsky, J. Grym, S. Kucerova, H. Faitova, R. Yatskiv, J. Vanis, J. Vesely and J. Maixner, Highly Textured Seed Layers for the Growth of Vertically Oriented ZnO Nanorods, *Crystals*, 2019, **9**, 566.

18 S. Abubakar, S. T. Tan, J. Y. C. Liew, Z. A. Talib, R. Sivasubramanian, C. A. Vaithilingam, S. S. Indira, W.-C. Oh, R. Siburian, S. Sagadevan and S. Paiman, Controlled Growth of Semiconducting ZnO Nanorods for Piezoelectric Energy Harvesting-Based Nanogenerators, *Nanomaterials*, 2023, **13**, 1025.

19 D. Sakai, K. Nagashima, H. Yoshida, M. Kanai, Y. He, G. Zhang, X. Zhao, T. Takahashi, T. Yasui, T. Hosomi, Y. Uchida, S. Takeda, Y. Baba and T. Yanagida, Substantial Narrowing on the Width of "Concentration Window" of Hydrothermal ZnO Nanowires *via* Ammonia Addition, *Sci. Rep.*, 2019, **9**, 14160.

20 R. Parize, J. D. Garnier, E. Appert, O. Chaix-Pluchery and V. Consonni, Effects of Polyethylenimine and Its Molecular Weight on the Chemical Bath Deposition of ZnO Nanowires, *ACS Omega*, 2018, **3**, 12457–12464.

21 E. Carlos, J. Leppäniemi, A. Sneck, A. Alastalo, J. Deuermeier, R. Branquinho, R. Martins and E. Fortunato, Printed, Highly Stable Metal Oxide Thin-Film Transistors with Ultra-Thin High-κ Oxide Dielectric, *Adv. Electron. Mater.*, 2020, **6**, 1901071.

22 M. Miyakawa, M. Nakata, H. Tsuji and Y. Fujisaki, Simple and reliable direct patterning method for carbon-free solution-processed metal oxide TFTs, *Sci. Rep.*, 2018, **8**, 12825.

23 E. Carlos, R. Branquinho, P. Barquinha, R. Martins and E. Fortunato, *Chemical Solution Synthesis for Materials Design and Thin Film Device Applications*, Elsevier, 2021, pp. 585–621.

24 J. Lin, *Printed Electronics*, John Wiley & Sons Singapore Pte. Ltd, Singapore, 2016, pp. 106–144.

25 J. Leppäniemi, O. Huttunen, H. Majumdar and A. Alastalo, Flexography-Printed In₂O₃ Semiconductor Layers for High-Mobility Thin-Film Transistors on Flexible Plastic Substrate, *Adv. Mater.*, 2015, **27**, 7168–7175.

26 K.-H. Lim, J. Lee, J.-E. Huh, J. Park, J.-H. Lee, S.-E. Lee and Y. S. Kim, A systematic study on effects of precursors and solvents for optimization of solution-processed oxide semiconductor thin-film transistors, *J. Mater. Chem. C*, 2017, **5**, 7768–7776.

27 T. Amakali, L. S. Daniel, V. Uahengo, N. Y. Dzade and N. H. de Leeuw, Structural and Optical Properties of ZnO Thin Films Prepared by Molecular Precursor and Sol–Gel Methods, *Crystals*, 2020, **10**, 132.

28 E. T. Seid and F. B. Dejene, Post-heat treatment effect on the properties of indium doped zinc oxide nanocrystals produced by the sol-gel method, *Opt. Mater. Express*, 2020, **10**, 2849.

29 M. C. M. Angub, C. J. T. Vergara, H. A. F. Husay, A. A. Salvador, M. J. F. Empizo, K. Kawano, Y. Minami, T. Shimizu, N. Sarukura and A. S. Somintac, Hydrothermal growth of vertically aligned ZnO nanorods as potential scintillator materials for radiation detectors, *J. Lumin.*, 2018, **203**, 427–435.

30 S. Henriques Ferreira, A. Rovisco, A. dos Santos, H. Águas, R. Igreja, P. Barquinha, E. Fortunato and R. Martins, in *Nanopores*, ed. S. Ameen, M. S. Akhtar and H.-S. Shin, IntechOpen, 2021.

31 A. dos Santos, F. Sabino, A. Rovisco, P. Barquinha, H. Águas, E. Fortunato, R. Martins and R. Igreja, Optimization of ZnO Nanorods Concentration in a Micro-Structured Polymeric Composite for Nanogenerators, *Chemosensors*, 2021, **9**, 27.

32 A. Pimentel, A. Samouco, D. Nunes, A. Araújo, R. Martins and E. Fortunato, Ultra-fast microwave synthesis of ZnO nanorods on cellulose substrates for UV sensor applications, *Materials*, 2017, **10**, 4–10.

33 J. Hong, K. Katsumata and N. Matsushita, High-conductivity solution-processed ZnO films realized *via* UV irradiation and hydrogen treatment, *Acta Mater.*, 2016, **103**, 844–849.

34 C.-L. Tsai, Y.-C. Tseng, W.-M. Cho, Y.-J. Lin, H.-C. Chang, Y.-H. Chen and C.-H. Lin, Effects of ultraviolet treatment on the optical and structural properties of ZnO nanoparticles, *Mater. Chem. Phys.*, 2011, **130**, 299–302.

35 W. Han, J. Kim and H.-H. Park, Control of electrical conductivity of highly stacked zinc oxide nanocrystals by ultraviolet treatment, *Sci. Rep.*, 2019, **9**, 6244.

36 M. Morais, M. Cortinhal, A. Rovisco, J. Martins, R. Martins and P. Barquinha, *Zinc Oxide Nanoparticles – Fundamentals and Applications*, IntechOpen, 2024.

37 L. Wang, X. Li, Q. Li, X. Yu, Y. Zhao, J. Zhang, M. Wang and R. Che, Oriented Polarization Tuning Broadband Absorption from Flexible Hierarchical ZnO Arrays Vertically Supported on Carbon Cloth, *Small*, 2019, **15**(18), 1900900.

38 S. S. A. Karim, C.-F. Dee, B. Y. Majlis and M. A. Mohamed, Recent Progress on Fabrication of Zinc Oxide Nanorod-based Field Effect Transistor Biosensors, *Sains Malays.*, 2019, **48**, 1301–1310.

39 M. Kamruzzaman and J. A. Zapien, Effect of Temperature, Time, Concentration, Annealing, and Substrates on ZnO Nanorod Arrays Growth by Hydrothermal Process on Hot Plate, *Crystallogr. Rep.*, 2018, **63**, 456–471.

40 Q. He and J. Briscoe, Piezoelectric Energy Harvester Technologies: Synthesis, Mechanisms, and Multifunctional Applications, *ACS Appl. Mater. Interfaces*, 2024, **16**, 29491–29520.

41 K. Kanuga, in 2011 37th IEEE Photovoltaic Specialists Conference, IEEE, 2011, pp. 000096–000100.

42 N. F. Nazari, M. Rajabi and A. Z. Moshfegh, The UV photodetection enhancement of tailored ZnO nanorods by controlling the aspect ratio, *Surf. Interfaces*, 2022, **28**, 101682.

43 A. Y. Al-She'irey, A. Balouch, E. R. Mawarnis, L. Roza, M. Y. A. Rahman, Abdullah and A. M. Mahar, Effect of ZnO seed layer annealing temperature on the growth of ZnO nanorods and its catalytic application, *Opt. Mater.*, 2022, **131**, 112652.

44 Y. Lee, N. Kaur, S. Choi, D. Y. Kim and S. Lee, A comprehensive study on structural, microstructural, and optical properties of YZnO nanorods prepared by seed morphology-controlled hydrothermal growth, *Appl. Surf. Sci.*, 2021, **556**, 149741.

45 C. Liu, Q. Tian and L. Liao, *Solution Processed Metal Oxide Thin Films for Electronic Applications*, Elsevier, 2020, pp. 41–61.

46 Y. Zhang, G. Lu, M. Chen, Y. Liu and R. Yao, Flexible Self-Powered Tactile Sensors Based on Hydrothermally Grown ZnO Nanorods, *IEEE Sens. J.*, 2022, **22**, 12613–12621.

47 A. J. L. Lopez Garcia, M. Mouis, V. Consonni and G. Ardila, Dimensional Roadmap for Maximizing the Piezoelectrical Response of ZnO Nanowire-Based Transducers: Impact of Growth Method, *Nanomaterials*, 2021, **11**, 941.

48 L. Zhu, Y. Xiang, Y. Liu, K. Geng, R. Yao and B. Li, Comparison of piezoelectric responses of flexible tactile sensors based on hydrothermally-grown ZnO nanorods on ZnO seed layers with different thicknesses, *Sens. Actuators, A*, 2022, **341**, 113552.

49 M. M. J. van Rijt, B. M. Oosterlaken, R. R. M. Joosten, L. E. A. Wijkhuijs, P. H. H. Bomans, H. Friedrich and G. de With, Counter-ion influence on the mechanism of HMTA-mediated ZnO formation, *CrystEngComm*, 2020, **22**, 5854–5861.

50 M. Abd-Ellah, N. Moghimi, L. Zhang, N. F. Heinig, L. Zhao, J. P. Thomas and K. T. Leung, Effect of Electrolyte Conductivity on Controlled Electrochemical Synthesis of Zinc Oxide Nanotubes and Nanorods, *J. Phys. Chem. C*, 2013, **117**, 6794–6799.

51 M. Kardeş and K. Öztürk, Photocatalyst ZnO nanorod arrays on glass substrates: the critical role of seed layer in nanorod alignment and photocatalytic efficiencies, *Chem. Eng. Commun.*, 2020, **207**, 1522–1535.

52 A. A. Hssi, L. Atourki, N. Labchir, M. Ouafi, K. Abouabassi, A. Elfanaoui, A. Ihlal and K. Bouabid, Electrodeposition of oriented ZnO nanorods by two-steps potentiostatic electrolysis: Effect of seed layer time, *Solid State Sci.*, 2020, **104**, 106207.

53 V. Consonni and A. M. Lord, Polarity in ZnO nanowires: A critical issue for piezotronic and piezoelectric devices, *Nano Energy*, 2021, **83**, 105789.

54 C. Lausecker, B. Salem, X. Baillin and V. Consonni, Effects of Zinc Nitrate and HMTA on the Formation Mechanisms of ZnO Nanowires on Au Seed Layers, *Cryst. Growth Des.*, 2023, **23**, 2941–2950.

55 V. Strano, R. G. Urso, M. Scuderi, K. O. Iwu, F. Simone, E. Ciliberto, C. Spinella and S. Mirabella, Double Role of HMTA in ZnO Nanorods Grown by Chemical Bath Deposition, *J. Phys. Chem. C*, 2014, **118**, 28189–28195.

56 S. Allami, *Nanowires – Synthesis, Properties and Applications*, IntechOpen, 2021.

57 M. Manrique, V. Consonni, S. Boubenia, H. Roussel, M. Zeghouane, S. Labau, S. Cavalaglio, C. Pudda, V. Jacob, G. Le Rhun and B. Salem, Enhancing the Output Voltage of Piezoelectric Nanogenerators Based on ZnO Nanowires Grown by Chemical Bath Deposition Using Compensatory Cu Doping, *Energy Technol.*, 2024, **12**(5), DOI: **10.1002/ente.202301381**.

58 D. Yang, Y. Qiu, Q. Jiang, Z. Guo, W. Song, J. Xu, Y. Zong, Q. Feng and X. Sun, Patterned growth of ZnO nanowires on flexible substrates for enhanced performance of flexible piezoelectric nanogenerators, *Appl. Phys. Lett.*, 2017, **110**(6), 063901.

59 A. Anand and M. C. Bhatnagar, Role of vertically aligned and randomly placed zinc oxide (ZnO) nanorods in PVDF matrix: Used for energy harvesting, *Mater. Today Energy*, 2019, **13**, 293–301.

60 H. Eom, J. Hur, S.-K. Sung, J.-H. Jeong and I. Park, Density-controlled electrochemical synthesis of ZnO nanowire arrays using nanotextured cathode, *Nanotechnology*, 2024, **35**, 185301.